國立臺灣大學生命科學學院生命科學系

碩士論文

Department of Life Science College of Life Science



National Taiwan University

Master Thesis

利用基因剃除技術研究藍綠菌Synechococcus sp. PCC 7335中可吸收 遠紅光的光系統一

Mutagenesis study of the Photosystem I that absorbs far-red light in a cyanobacterium *Synechococcus* sp. PCC 7335

陳楷文

Kai-Wen Chen

指導教授: 何銘洋 助理教授

Advisor: Ming-Yang Ho, Assistant Professor

中華民國 111年 08月

August 2022

口試委員審定書



國立臺灣大學碩士學位論文 口試委員會審定書

利用基因剃除技術研究藍綠菌 Synechococcus sp. PCC 7335 中可吸收遠紅光的光系統一

Mutagenesis study of the Photosystem I that absorbs far-red light in a cyanobacterium *Synechococcus* sp. PCC 7335

本論文係陳楷文君 (R09B21026) 在國立臺灣大學生命 科學系、所完成之碩士學位論文,於民國 111 年 8 月 17 日 承下列考試委員審查通過及口試及格,特此證明

| 口試委員: | | 15 | 似当 | (| (簽名) |
|-------|---------|-------|----------|-----------|------|
| | 24 | りか(指) | 導教授) | | |
| | | 獅孩 | | | |
| | <u></u> | (11) | | | |
| 生命科學系 | 系主任 | 黃 | 偉邦 |) (簽名) |)_ |

致謝

能夠順利完成這一篇論文,首先要感謝的是我的指導教授—何銘洋老師。在這兩年的碩士班生涯中,給與我許多的幫助,包括實驗上以及論文寫作上,老師皆能夠以循循善誘的方式引導我走在對的道路上。藉由定期的進度報告檢驗實驗進度的同時搭配上定期的期刊文獻分享報告來吸收新知,在這樣的步調中,使我對於原本不熟悉的藍綠菌領域的研究有了更多的認識以及熟稔相關實驗的操作來完成論文。

此外也很感謝朱修安、謝旭亮、傳輸儀老師在口試時以及口試後提供許多建議幫助我來編撰修改我的論文使其更加完善。另外也要感謝實驗室的同仁在這兩年期間提供許多實驗技術性上以及寫作上的建議,在我徬徨無措的時候鼓勵我繼續完成這一篇論文。

最後,要感謝我的家人,在背後不斷的支持我當我最堅強的後盾使我可以專心 在我的研究以及寫作上面,感謝你們!

Table of contents

| 口言 | 試委員審定書 | i A |
|-------------|--|------------------------------------|
| 致記 | 谢 | ii ii |
| Tab | ole of contents | iii |
| ΑI | List of Figures | vi |
| ΑI | List of Tables | vii |
| 摘 | 要 | viii |
| Ab | stract | ix |
| 1. | Introduction | 1 |
| 2. I | Material and methods | 4 |
| | 2.1 Cyanobacterial strains and growth conditions | 4 |
| | 2.2 Cargo plasmid building up | 4 |
| | 2.3 Conjugative transformation and homologous recomb | ination in |
| | Synechococcus sp. PCC 7335 | 5 |
| | 2.4 Absorption spectroscopy and room temperature and | low-temperature |
| | (77K) fluorescence spectroscopy | 6 |
| | 2.5 Pigments extraction and HPLC analysis | 7 |
| | 2.6 Isolation of trimeric PSI complexes | 8 |
| 3. I | Results | 9 |
| | 3.1 Conjugants built up | 9 |
| | 3.2 The comparisons of growth rates | 9 |
| | 3.3 Absorption spectra of Syn7335 WT, psaF2-, psaI2-, ps | <i>aJ2</i> -, <i>psaL2</i> - cells |
| | grown under FRL | 10 |
| | 3.5 Photosystem I isolation of WT and mutants (psaF2*, p | osaI2-, psaJ2-, psaL2-) |
| | | 12 |

| 3.6 High-Performance Liquid Chromatography (HPLC) of the FRL Syn7335- | 100 |
|---|-----|
| WT and mutants' (psaF2-, psaI2-, psaJ2-, psaL2-) cells and their isolated PSI 1 | 3 |
| 3.7 Absorbance spectra and fluorescence spectra of isolated PSI complexes . 1 | 4 |
| 4. Discussion | 5 |
| 4.1 The blue shift of psaF2 and psaJ2 under RT and 77K fluorescence | |
| spectrum | 5 |
| 4.2 The Chl f binding site specification near PsaJ2 | 6 |
| 4.3 PSI structure changes in $psal2^-$ and $psal2^-$ and the exploration of Chl f | |
| binding abilities1 | 7 |
| 5. Conclusion and future works | 8 |
| Figures | 0 |
| Fig. 1 Protein and pigments absorption spectra and the structure of | |
| chlorophylls2 | 0 |
| Fig. 2 Regulation mechanism of FaRLiP. | 1 |
| Fig. 3 Possible Chl f binding sites based on the cryogenic electron microscopy | |
| (cryo-EM) data from (C. J. Gisriel et al., 2022; C. J. Gisriel et al., 2020) 2 | 2 |
| Fig. 4 Cargo plasmids are designed for conjugal transformation, and the | |
| colony PCR results of conjugation | 3 |
| Fig. 5 Growth curve of Syn7335 WT and mutants under WL and FRL 2 | 4 |
| Fig. 6 The doubling time of the FRL Syn7335-WT and the four mutants | |
| (psaF2-, psaI2-, psaJ2-, and psaL2-) cells | 5 |
| Fig. 7 Syn7335 WT and mutants' (psaF2-, psaI2-, psaJ2-, and psaL2-) | |
| absorption spectra2 | 6 |
| Fig. 8 The RT fluorescence spectrum of the FRL Syn7335-WT and the four | |
| mutants (nsaF2-, nsaI2-, nsaI2-, nsaI.2-) cells | 7 |

| Fig. 9 Isolation of PSI complexes from Syn7335-WT and psaF2-, psaI2-, psaJ2-, |
|---|
| psaL2 ⁻ cells |
| Fig. 10 The chlorophyll ratio of Chl a: Chl d: Chl f in the 100 % stacked bar |
| chart of FRL Syn7335-WT, psaF2-, psaJ2- cells |
| Fig. 11 The chlorophyll ratio of Chl a : Chl d : Chl f in the 100 % stacked bar |
| chart of the trimeric PSI purified from FRL Syn7335-WT, psaF2-, psaJ2 30 |
| Fig. 13 RT fluorescence spectra of Syn7335 WT, psaF2-, psaJ2- PSI trimer 32 |
| Fig. 14 77K fluorescence spectrum of Syn7335 WT, psaF2-, psaJ2- PSI trimer. |
| |
| Tables |
| Table 1 Medium solution of ASN-III liquid and plate |
| Table 2 Primers used in this study |
| References |
| Appendix49 |
| Appendix 1 Absorbance spectra of the mutants and WT cells grown under |
| FRL |
| Appendix 2 The chlorophyll ratio of Chl a: Chl d: Chl f in the 100 % stacked |
| bar chart of FRL Syn7335-WT, psaF2-, psaI2-, psaJ2-, and psaL2- cells 50 |

A List of Figures

| Fig. 1 Protein and pigments absorption spectra and the structure of |
|--|
| chlorophylls20 |
| Fig. 2 Regulation mechanism of FaRLiP. |
| Fig. 3 Possible $Chl f$ binding sites based on the cryogenic electron |
| microscopy (cryo-EM) data from (C. J. Gisriel et al., 2022; C. J. |
| Gisriel et al., 2020) |
| Fig. 4 Cargo plasmids are designed for conjugal transformation, and the |
| colony PCR results of conjugation |
| Fig. 5 Growth curve of Syn7335 WT and mutants under WL and FRL. 24 |
| Fig. 6 The doubling time of the FRL Syn7335-WT and the four mutants |
| (psaF2 ⁻ , psaI2 ⁻ , psaJ2 ⁻ , and psaL2 ⁻) cells |
| Fig. 7 Syn7335 WT and mutants' (psaF2-, psaI2-, psaJ2-, and psaL2-) |
| absorption spectra |
| Fig. 8 The RT fluorescence spectrum of the FRL Syn7335-WT and the |
| four mutants (psaF2-, psaI2-, psaJ2-, psaL2-) cells |
| Fig. 9 Isolation of PSI complexes from Syn7335-WT and psaF2-, psaI2-, |
| psaJ2 ⁻ , psaL2 ⁻ cells |
| Fig. 10 The chlorophyll ratio of Chl a: Chl d: Chl f in the 100 % stacked |
| bar chart of FRL Syn7335-WT, psaF2-, psaJ2- cells |
| Fig. 11 The chlorophyll ratio of Chl a: Chl d: Chl f in the 100 % stacked |
| bar chart of the trimeric PSI purified from FRL Syn7335-WT, |
| <i>psaF2</i> -, <i>psaJ2</i> |
| Fig. 12 Absorbance spectra of Syn7335 WT, $psaF2$ -, $psaJ2$ - PSI trimer 31 |
| Fig. 13 RT fluorescence spectra of Syn7335 WT, psaF2-, psaJ2- PSI |
| trimer |
| Fig. 14 77K fluorescence spectrum of Syn7335 WT, psaF2-, psaJ2- PSI |
| trimer |
| Appendix 1 Absorbance spectra of the mutants and WT cells grown |
| under FRL |
| Appendix 2 The chlorophyll ratio of Chl a: Chl d: Chl f in the 100 % |
| stacked bar chart of FRL Syn7335-WT, psaF2-, psaI2-, psaJ2-, and |
| psaL2- cells |

A List of Tables

| Table 1 Medium solution of ASN-III liquid and plate | | 34 |
|--|------------|-------|
| Table 1 Medium solution of ASN-III liquid and plate Table 2 Primers used in this study | New Market | 36 |
| Table 2 11 miers assu in onis soudy | 47 3 | 3. 壁柳 |

摘要

大部分的光合生物可以利用波長 400-700 奈米的可見光能源。然而,有一些品種的 藍綠菌除了可以利用 400-700 nm 波長的能源外,也可以利用遠紅光 (波長 700-800 奈米)。當生活在可見光較少且遠紅光較多的環境時,它們可以行遠紅光轉換作用 來適應環境。經由遠紅光轉換,這些藍綠菌會產生葉綠素d、f,以及表現遠紅光基 因簇中的 20 個基因來重組光系統一、二以及藻膽蛋白體。近期冷凍電子顯微鏡解 出的藍綠菌遠紅光下的光系統一結構,揭露了幾個可能的葉綠素f結合位點。然而, 葉綠素 f 以及葉綠素 a 結構上非常相似,因此以目前的技術要能夠直接區分出兩者 具有非常大的挑戰性,在一些解析度比較侷限的區域上更是不容易確定。並且,每 個葉綠素f在光系統一中所扮演的角色也不清楚。為了彌補結構研究上的不足,我 們選定了在遠紅光光系統一中坐落在可能葉綠素f結合位點附近的四個基因(psaF2,12, J2, and L2)來進行基因剃除。結果顯示 psaL2 突變株不但在遠紅光下長得比較 慢,而且同時他們的葉綠素f:a比例也降低了。此外我們也發現缺少PsaF2和PsaJ2並不會影響到光系統一的三聚體結構,但卻會改變光譜特性。再者,結合先前的結 構研究以及以高效液相層析測量得出的結果-在遠紅光下突變株psaJ2光系統I中 的葉綠素f含量比率和野生株以及突變株psaF2-的光系統I中的含量來的低可以推 斷出,在蛋白為單元體 PsaJ2 附近有一個葉綠素 f 的結合位。

關鍵字: 遠紅光轉換, 基因剔除, 螢光光譜學, 吸收光譜學

Abstract

Most oxygenic phototrophs use photosynthetically active radiation (PAR; wavelengths = 400-700 nm) for photosynthesis. However, some special cyanobacteria can use PAR and far-red light (FRL, wavelengths = 700-800 nm). When these cyanobacteria grow in FRLenriched environments, they perform far-red light photoacclimation (FaRLiP) to harvest FRL. While performing FaRLiP, they synthesize chlorophyll d (Chl d) and chlorophyll f (Chl f) and express 20 genes in the FaRLiP gene clusters to remodel their photosystem I (PSI), photosystem II, and also phycobilisome. Recent PSI structural cryogenic electron microscopy (cryo-EM) studies identified several possible Chl f binding sites in the FRLremodeled PSI. However, the structure of Chl f and Chl a are too similar, and in some regions with lower resolution, they are hard to differentiate under the resolution of cryo-EM. In addition, the function of each Chl f molecule in PSI is still unknown. To complement the deficiency of cryo-EM, we individually used conjugation and homologous recombination to knockout the four PSI subunits (PsaF2, I2, J2, and L2) in the FaRLiP gene cluster in Synechococcus sp. PCC 7335. These four subunits are near the proposed binding sites in the cryo-EM structure. We found that the psaI2⁻ and psaL2⁻ mutant grows slower than the wild type under FRL and decreases the Chl f: a ratio. Also, the PSI purification result shows that the lack of PsaF2 or PsaJ2 does not affect trimerization but changes the spectral properties of the complex. Moreover, combined with previous structural studies and the HPLC analysis that the Chl f molecules ratio is decreased in the purified FRL PSI of psaJ2⁻, there is a Chl f binding site near PsaJ2.

Keywords: far-red light photoacclimation (FaRLiP), gene knockout, fluorescence spectroscopy, absorption spectroscopy

1. Introduction

On earth, all photoautotrophs can acquire energy from the sun and transform the inorganic compounds into organic compounds as food sources to survive. Photoautotrophs can be further classified into monoplast and multicellular organisms. Among all the photoautotrophs, cyanobacteria are the most primitive and have simple physiological regulation mechanisms, becoming one of the best model organisms to study physiological mechanisms and gene regulations (Whitton, 2012). When cyanobacteria grow in the wild, they will encounter many survival competitions to strive for limited sources such as light, carbon, and organic compounds. In the competition process, superior cyanobacteria can occupy the upper niche close to the top of the surroundings to acquire more light sources. Instead, some cyanobacteria that are not superior to others can only live in deeper places that have a limited visible light source. (Kardinaal et al., 2007) However, under this circumstance that the far-red light can reach a deeper region (Gan & Bryant, 2015). And that is this situation that caused the cyanobacteria to evolve the capability to use far-red light, which is later named far-red light photoacclimation (Gan et al., 2014; Wolf & Blankenship, 2019), to help them acclimate to an environment that has more far-red light (FRL) and less photosynthetically active radiation (PAR; 400 – 700 nm).

In this study, a cyanobacterial strain, *Synechococcus* sp. PCC 7335, which can perform far-red light photoacclimation (FaRLiP), was chosen to investigate the FaRLiP mechanism. (Ho et al., 2017). When the cyanobacteria which can conduct FaRLiP grows under an environment having more FRL and PAR, the P_{fr} form of RfpA would receive the light and then activate the downstream FaRLiP gene cluster and express 20 genes to remodel the photosystem II (PSII), photosystem I (PSI), and phycobilisome. Also, when the cyanobacteria which can perform FaRLiP acclimated to far-red light, they can produce chlorophyll d (Chl d) and chlorophyll f (Chl f) (Ho et al., 2016). And Chl d and Chl f

molecules can bind to the remodeled PSI and PSII and help the cyanobacteria acquire farred light energy. With the help of Chl d and Chl f molecules binding in the proper position on PSII and PSI, cyanobacteria can use the FRL energy efficiency and make them able to survive (Chen et al., 2002; C. Gisriel et al., 2020).

Based on previous studies, the enzyme capable of producing Chl f molecules was found (Ho et al., 2016), but the binding sites of the Chl f molecules were unclear. Also, because each photon of FRL energy is less than the photon that comes from PAR, identifying the locations of Chl f molecules is a vital issue in knowing the uphill energy transfer steps and the mechanism of FaRLiP. In the previous studies, the Brudvig group from Yale University used cryogenic electron microscopy (cryo-EM) to identify the PSI structure fully acclimated to FRL (Christopher Gisriel et al., 2020; Christopher J. Gisriel, David A. Flesher, et al., 2022; Gisriel et al., 2021). Based on their cryo-EM data, the authors proposed several possible Chl f molecules binding sites in their protein complexes' results. However, the slight functional differences between Chl a and Chl f molecules, which have a methyl group on the C2 position and a formyl group, make them hard to differentiate under cryo-EM (fig. 1B, 1C). Also, when the cyanobacteria perform FaRLiP, the FaRLiP gene cluster would be expressed, among them, six PSI genes (psaA2, psaB2, psaF2, psaI2, psaJ2, and psaL2) would remodel PSI to help the cyanobacteria live under this condition (fig. 2).

In this study, some subunits (PsaF2, PsaI2, PsaI2, PsaI2) near the possible Chl f molecules binding sites were chosen to do the mutagenesis to identify the potential critical areas of Chl f molecules (**fig. 3**). The knockout mutants were further examined by colony PCR and sent for sequencing. After that, they were cultured in a liquid ASN-III medium for growth curve, absorbance spectrum, and fluorescence spectrum measurements. In the growth curve measurement, $psaI2^-$ and $psaL2^-$ show that they have a longer doubling time

than Synechococcus sp. PCC7335 (Syn7335) wild-type (WT) and psaF2 and psaJ2 in far-red light. And the two mutants (psal2 and psaL2) also have lower fluorescence emission and FRL absorbance ability than Synechococcus sp. PCC7335 wild-type and psaF2⁻ and psaJ2⁻ in far-red light under fluorescence and absorbance spectra. After that, the four mutants (psaF2-, psaI2-, psaJ2-, and psaL2-) and WT were cultured in large volumes to further PSI isolation. PSII and PSI were purified and separated with a 5-20% sucrose gradient. The isolation results show that PSI trimer only can be found from FRL Syn7335-WT, psaF2⁻, psaJ2⁻ but not on psaI2⁻ and psaL2⁻. The further PSI trimers purified from the FRL Syn7335-WT, psaF2⁻, and psaJ2⁻ were used to detect the protein complexes' absorbance and fluorescence spectra and the HPLC analysis. In the absorbance and fluorescence spectrum, psaF2 and psaJ2 have a blue shift Qy peak compared with FRL-WT PSI. And the peak height of around 730 nm of psaJ2 seems to be higher than that of psaF2 under the room-temperature (RT) fluorescence spectrum. Besides, psaI2⁻ and psaL2⁻ did not have a band containing a trimeric structure of PSI. This result is similar to a previous study that knocked out white light type psal2 and psaL2 (Schluchter et al., 1996). In the HPLC analysis, the Chl f content seems to be the same between the cells' FRL-WT, psaF2-, and psaJ2. However, the Chl f ratio is lower in the purified PSI of psaJ2⁻. In this study, we found that knockout of psaI2 and psaL2 would affect the growth of Syn7335 under FRL but not under WL. Second, knockout of psaI2 or psaL2 would affect the PSI structure of Syn7335 under FRL and cause trimeric PSI cannot be generated. Third, combined with the previous structural study and the HPLC analysis, there is a Chl f binding site around PsaJ2.

2. Material and methods

2.1 Cyanobacterial strains and growth conditions

The cyanobacteria strain *Synechococcus* sp. PCC 7335 (Syn7335) was taken from Pasteur Culture Collection Center (www.pasteur.fr/en/pcc). Syn7335 originated on the snail shell in the intertidal zone close to Puerto Penasco, Mexico (Rippka et al., 1979). The strain was cultured in ASN-III medium replenished with vitamin B₁₂ (4 mg L⁻¹) and 10 mM Tris–HCl, pH 8.0 at 30°C, supplemented with 1% (v/v) CO₂. The composition of the modified ASN-III medium is shown in **appendix table 1**. Continuous illumination of white LED light (HiPoint, Taiwan) with ~100 μmol photons m⁻² s⁻¹ and far-red LED light (HiPoint, Taiwan) with ~100 μmol photons m⁻² s⁻¹ (centered at 730 nm) were used as the light sources to culture the cyanobacteria.

2.2 Cargo plasmid building up

The plasmid pRL277 was double cut by SphI, and the digested product with 5901bp was set as the cargo plasmid backbone. BamHI and SpeI digested the pJET-km, and the *aphAII* resistant cassette was used as the insert. The other two inserts of the cargo plasmid on the target genes' upstream and downstream 3 kb of Syn7335 genomic DNA were amplified with the primer containing 29-30 bp overhang with digested pRL277 backbone and *aphAII* resistant cassette. Then the four segments were assembled by the HIFI DNA assembly (NEB, USA), and the product was used to transform into *E. coli* DH5α. All of the primers used for the construct building up are shown in **appendix table 2.**

2.3 Conjugative transformation and homologous recombination in *Synechococcus* sp. PCC 7335

The system of conjugation exerted on Synechococcus sp. PCC 7335 was adapted from previous studies with slight changes (Zhao et al., 2015; Zhao et al., 2005). DNA fragments (~3 kb) from the upstream and downstream flanking region of the target gene (psaF2, psaI2, psaJ2, psaL2) were amplified by polymerase chain reaction (PCR). And the aphAII encoding kanamycin-resistant cassette was digested with BamHI and SpeI from the plasmid of pJET-km. Also, a ~7kb fragment taken from pRL277 was digested with SphI and set as the backbone of the cargo plasmid. All four segments were linked with HIFI DNA assembly (NEB, USA) into one intact cargo plasmid. The cargo plasmids were further transformed into Escherichia coli HB101 competent cells containing conjugal plasmid pRL443 and helper plasmid pRL623 (Elhai et al., 1997; Elhai & Wolk, 1988). E. coli cells were cultured at 37°C for 16-18 h in 20 mL of Luria-Bertani (LB) medium supplemented with 100 mg ampicillin L⁻¹, 50 mg chloramphenicol L⁻¹, 100 mg spectinomycin L⁻¹, 12.5 mg tetracycline L⁻¹, and 100 mg kanamycin L⁻¹. 20 mL of E. coli culture and 5 mL of Synechococcus sp. PCC 7335 cells (OD_{750 nm} = 0.4-0.8) were centrifugated at 5510 x g for 5 min. E. coli cell pellets were washed with LB medium twice, ASN-III medium once, and Synechococcus sp. PCC 7335 cell pellets were washed with ASN-III medium three times. After washing the cell pellets, Synechococcus sp. PCC 7335 cells pellets were resuspended with 200 µL of ASN-III medium. Further, the solution containing Syn7335 cells was used to resuspend the E. coli cell pellets. Then the mixtures were left at room temperature for 4-6 h under low light and streaked on a sterile nitrocellulose filter (diameter = 47 mm; pore size = 0.45 μm, PALL, USA) overlaid on a 1.5% (w/v) ASN-III agar plate. After staying under low light for two days, the nitrocellulose membrane was transferred to a 1.5% (w/v) ASN-III agar plate

supplemented with kanamycin (100 mg L⁻¹). After colonies became observable on the plate, they were picked up and streaked on a new ASN-III plate supplemented with kanamycin (100 mg L⁻¹). Colony PCR using the primers, which amplified partly of the upstream and downstream flanking region of the target gene covered with *aphII* antibiotic-resistant cassette, was performed to confirm the genetic knockout of the conjugants.

2.4 Absorption spectroscopy and room temperature and low-temperature (77K) fluorescence spectroscopy

WT and mutant strains (psaF2⁻, psaI2⁻, psaJ2⁻, psaL2⁻) of Syn7335 were cultured in WL and FRL until the OD_{750 nm} values reached 0.5-1.0. Aliquots of cells were collected by centrifugation with 10000 x g for 2 min. An Agilent spectrometer (Cary 60, Agilent, USA) detected the OD_{750 nm} value, and the cell density was adjusted to OD_{750 nm} = 0.2 with a total volume of 1 mL in a modified ASN-III medium to measure the absorption spectrum for cells with MAPADA (UV-1800, China). On the other hand, to measure the absorption spectrum of the purified proteins, the purified protein products were dissolved in MES buffer (50 mM MES, pH 6.5, 10 mM CaCl₂, and 10 mM MgCl₂) with absorbance between 400-700 nm less than 1.0, and the spectrum was detected by Agilent spectrometer. The fluorescence spectra were all measured with the Hitachi F7000 fluorometer (Hitachi, Japan), but the protocols were slightly different when detecting cells and purified protein products. The machine was set at a PMT voltage of 700V with an excitation slit and emission slit of 5 nm. All the fluorescence spectra were detected with a scan speed of 240 nm min⁻¹. The cell density was also adjusted to $OD_{750 \text{ nm}} = 0.2$ with a total volume of 2 mL in a modified ASN-III medium to measure the room temperature fluorescence spectrum of the cells. Instead, the chlorophyll concentration was adjusted to $10~\mu g~mL^{-1}$

in MES buffer to measure the room temperature spectrum of purified proteins. The cells were centrifugated into pellets in microcentrifuge tubes first, and then 500 μL of modified ASN-III medium was used to resuspend the cells. 500 μL of 30 % (w/v) PEG as a cryoprotectant was added for 77K fluorescence spectroscopy. To measure purified protein 77K fluorescence spectrum, the PSI should be dissolved in 50 mM MES buffer, and the total chlorophyll concentration should reach 30 μg/mL in 60% glycerol (v/v) solution.

2.5 Pigments extraction and HPLC analysis

Cyanobacteria cells were centrifugated with 13000 x g for 2 min to collect cell pellets. The upper layer supernatant was discarded, and then the cell pellets were washed with 10 mM Tris-HCl, pH 8, once and then centrifugated with 13000xg for 2 min to remove the supernatant. After that, the cell pellets were added with 270 µL of acetone/methanol (7:2, v/v) and vortexed for 2 min to resuspend the pellets and mix with the solution thoroughly. Later, the solution should be centrifugated to remove the cell debris, and then the supernatant was left and then filtrated with a 0.2 µm pore size of polytetrafluoroethylene membrane syringe filter (PALL, USA). The flow-through solution was added with 1/10 volume of 1M ammonium acetate (NH₄OAc) and then transferred into the vials with caps. A JASCO PU-4180 RHPLC system (JASCO, Japan), matched with an analytical Discovery C18 column (25 cm x 4.6 mm) (KANTO CHEMICAL, Japan), was used to analyze the pigments. The method of reversed-phase HPLC analysis was performed as previously described (Gan & Bryant, 2015; Gan et al., 2014; Ho et al., 2016; Zhao et al., 2015).

2.6 Isolation of trimeric PSI complexes

As previously described, PSI complexes were isolated from the cells grown in FRL (Christopher Gisriel et al., 2020; Kurashov et al., 2019; Shen et al., 2019). The cells were collected by centrifugation at 10000 x g for 10 min and then washed with 50 mM Tris, pH 8 twice. The cells were then resuspended with 13 mL of MES buffer. The cells pellets were then added into a bead beater container with 0.05 mm and 0.01 mm glass beads with 1/4 volume of the cell solution and underwent beating by a bead-beater (BioSpec Products, USA) with [2 min beating, 1 min break] x 6 cycles. After six cycles of bead beating, the solution was transferred to 50 mL falcon tubes for centrifugation (10000 xg, 5 min) to remove cell debris. And then, the supernatant was further transferred into a 13PA centrifuge tube (Hitachi, Japan) and underwent ultracentrifugation with 126100 x g (CR22N, Hitachi, Japan) at 4°C for 30 min to collect the thylakoids. After centrifugation to remove sizeable insoluble debris, the thylakoid membrane was dissolved with 3 mL of MES buffer and then homogenized with Potter-Elvehjem homogenizer. The homogenized membrane was then transferred into a 15 mL centrifuge tube and added n-dodecyl-β-Dmaltoside (β -DM) until 1% of the total solution (v/v). The homogenized membrane was then continuously rotated for 1 h at 4 °C. After solubilization, the solution was further centrifuged to remove the insolubilized membrane and loaded onto a 40 PA centrifuge tube (Hitachi, Japan) containing (5 – 20% (w/v) sucrose, 0.01% β-DM (v/v)) sucrose gradient for 139000 x g, 18 h, 4°C ultracentrifugation (CR22N, Hitachi, Japan). Greencolored, chlorophyll-containing fractions representing trimeric FRL-PSI were collected and dialyzed against MES buffer. The dialyzed membrane was concentrated with a 30 kDa concentrator (Sartorius, Germany), and further dimethyl sulfoxide (0.5% (v/v)) and glycerol (10% v/v) were added to the purified complexes for crypto conservation. The samples were stored at -80°C until further spectroscopy and pigment analyses.

3. Results

3.1 Conjugants built up

The cyanobacteria *Synechococcus* sp. PCC 7335 (Syn7335) wild-type (WT) strain was set as the PCR template to amplify the target genes' upstream and downstream 3 kb segments. And these two flanking segments were linked with kanamycin-resistant cassette *aphAII* and pRL277 backbone to form thorough cargo plasmids, as shown in **fig. 4A**. Later, the cargo plasmids targeting *psaF2*, *psaI2*, *psaJ2*, and *psaL2* were utilized to do homologous recombination in Syn7335 and then replace the target genes with kanamycin-resistant cassette *aphAII* as shown in **fig. 4A**. Further, the conjugants were specified with primers amplified partly of the flanking region of target genes covered with *aphAII* antibiotic resistant cassette as shown in **fig. 4B**. And in **fig. 4C**, the knockout mutants of *psaF2*, *psaI2*, *psaJ2*, *and psaL2* were generated and verified.

3.2 The comparisons of growth rates

After the specification of colony PCR, each of the three correct conjugants of the mutants was picked up as three independent clones representing each mutant for growth curve and doubling time measurements. The growth curves shown in **fig. 5** indicate the growth curves of Syn7335 WT and the mutants $psaF2^-$, $psaJ2^-$, $psaJ2^-$, and $psaL2^-$ under visible light (WL) and far-red light (FRL), respectively. As the curves show, all the groups seem to have similar growth rates under WL, but $psaJ2^-$ and $psaL2^-$ had a slower growth rate than WT, $psaF2^-$, and $psaJ2^-$ under the FRL condition. **Fig. 6** shows that the doubling time of $psaJ2^-$ and $psaJ2^-$ have a longer time to double their cell number when compared with other mutants and WT. Also, the doubling time of the Syn7335 WT shows a significant difference in statistics (p-value < 0.05, Kruskal Wallis test) compared with $psaJ2^-$ and $psaL2^-$ under FRL. This result indicated that losing PsaI2 or PsaL2 would be

critical to the growth of Syn7335 while growing in FRL.

3.3 Absorption spectra of Syn7335 WT, psaF2-, psaI2-, psaI2-, psaI2- cells grown under FRL

In the absorption spectra (**fig. 7A**) of the FRL cells, $psaF2^-$ and $psaJ2^-$ have higher FRL absorbance peaks around 710 nm compared with FRL-WT, $psaI2^-$ and $psaL2^-$ group. However, the height differences between $psaF2^-$, $psaJ2^-$ toward WT are lower than those between $psaF2^-$, $psaJ2^-$ toward $psaI2^-$ and $psaL2^-$ near the FRL absorption region around 710 nm. Also, the curves are further normalized to a peak of 679 nm (**fig. 7B**). The results are similar to **fig. 7A** and have a slight difference in the $psaI2^-$ absorbance spectrum curve. After normalized to a peak point of 679 nm, which is the maximum absorbance peak of Chl a, the curve of $psaI2^-$ shift to a higher status and has the same height as FRL-WT of the FRL absorption peak around 710 nm. And for the absorption spectra covering the whole range from 400 - 800 nm of Syn7335 WT, $psaF2^-$, $psaI2^-$, $psaJ2^-$, and $psaL2^-$ are shown in **appendix 1**.

3.4 Room temperature fluorescence spectra of FRL Syn7335 WT, psaF2-, psaI2-, psaJ2-, psaL2- cells excited at 440 nm.

As shown in **fig. 8**, the whole cell room temperature (RT) fluorescence spectrum of *psaF2*-has the highest peak at 730 nm, which is the emission from Chl *f*. And the amplitude of the fluorescence level at 730 nm from top to bottom is *psaJ2*-, WT, *psaI2*-, and the least *psaL2*-. The low Chl *f* emission of *psaI2*- and *psaL2*- indicates that knocking out *psaI2* or *psaL2* may affect the PSI structure and energy transfer. The other possibility is that the sites of Chl *f* molecules are located near PsaI2 or PsaL2, and knocking out these two subunits would reduce the peak height of Chl *f* emission. The PSI isolation experiments were further executed to clarify the possibility that losing trimeric PSI would cause a decrease in the emission peak height of Chl *f* molecules of *psaI2*- and *psaL2*-.

3.5 Photosystem I isolation of WT and mutants (psaF2-, psaI2-, psaI2-, psaI2-, psaL2-)

Fig. 9 shows the PSII and PSI from the FRL Syn7335-WT, and the four mutants (*psaF2*⁻, *psaI2*⁻, *psaJ2*⁻, *psaJ2*⁻, *psaJ2*⁻) were purified. In the first stage of purification, the cells were broken by a mixture of 0.1 and 0.5 mm glass beads, centrifuged down to remove insoluble debris, and loaded into the centrifuge tube for further ultra-high-speed centrifugation.

The first ultra-high-speed centrifugation results show that the supernatant's color contains

phycobiliproteins in centrifuge tubes of WT and the four mutants (*psaF2*-, *psaI2*-, *psaJ2*-, *psaJ2*-) are the same. The color of the supernatant in tubes is bluish, which is the typical color of FRL-type phycobilisomes that loss their phycoerythrin rods.

Further, the thylakoids were solubilized and underwent a second round of ultra-high-speed centrifugation to isolate the photosystem complexes. The isolation results are shown in **fig. 9**. The trimeric structure of PSI can only be found in FRL-WT, *psaF2*⁻ and *psaJ2*⁻ but not *psaI2*⁻ and *psaL2*⁻ (Kurashov et al., 2019). This result corresponds with previous whole cell absorption spectra (**fig. 7**) and the RT fluorescence spectra data excited with 440 nm (**fig. 8**). In the spectral data, the FRL absorbance peak and Chl *f* emission of *psaI2*⁻ and *psaL2*⁻ were vastly decreased compared with FRL-WT, *psaF2*⁻, and *psaJ2*⁻. To summarize, PsaI2 and PsaL2 participate in forming the trimeric structure of PSI, and also losing PsaI2 or PsaL2 would cause a decrease of Chl *f* molecules located nearby (C. J. Gisriel et al., 2022).

3.6 High-Performance Liquid Chromatography (HPLC) of the FRL Syn7335-WT

and mutants' (psaF2-, psaI2-, psaJ2-, psaL2-) cells and their isolated PSI

In **fig. 10** shows the ratios of the three chlorophylls (Chl a, Chl d, and Chl f) in the 100 % stacked bar chart. The percentage of Chl a: Chl d: Chl f is similar between FRL-WT, psaF2, and psaJ2 cells. And for the cells' HPLC results of the FRL Syn7335-WT and mutants,' (psaF2, psaJ2, psaJ2, psaJ2) cells are shown in **appendix 2**. In appendix 2, psaJ2 and psaJ2 have lower Chl f content than FRL Syn7335-WT, psaF2 and psaJ2. However, the ratio of Chl a: Chl d: Chl f shows a different trend between the trimeric structure PSI of FRL Syn7335-WT, psaF2, and psaJ2. As in **fig. 11** shown, the psaJ2 had the lowest Chl f molecules ratio between the trimeric structure PSI of FRL Syn7335-WT, psaF2, and psaJ2. Since each monomer of the FRL Syn7335-WT PSI has 92 chlorophylls, and chlorophyll site at B30 was proposed to be Chl f binding site close to PsaJ2 (Christopher J. Gisriel, David A. Flesher, et al., 2022). The Chl f content decreased by ~1 % in trimeric PSI of psaJ2 calculated from the HPLC compared with FRL Syn7335-WT and psaF2. Then the HPLC of the PSI trimeric structure can serve as another evidence to support that B30 is a Chl f binding site when specification on the mutant of psaJ2.

3.7 Absorbance spectra and fluorescence spectra of isolated PSI complexes

As **fig. 12** shown, the absorption spectra of the PSI trimer of FRL Syn7335-WT, *psaF2*, and *psaJ2*⁻ are very similar in the far-red light absorbance region (700 – 750 nm). The Chl *a* absorbance peak around 680 nm has a slight difference of *psaF2*⁻ which has a blue shift band peaked at 676.5 nm compared with FRL Syn7335-WT and *psaJ2*⁻, which had a peak near 680 nm. And in the RT fluorescence spectra excited at 440 nm shown in **fig. 13**, the blue shift happening in the Chl *f* emission is evident that the trimeric structure of *psaF2*⁻ and *psaJ2*⁻ has Chl *f* emission peak at 738 nm and 737 nm, respectively. Also, the emission peak height of *psaJ2*⁻ is lower than the emission peak of trimeric PSI of FRL Syn7335-WT. As for the 77K fluorescence spectra (**fig. 14**) of the purified trimeric PSI of Syn7335-WT, *psaF2*⁻, and *psaJ2*⁻, the phenomenon of blue-shifted emission peaks can also be found in the trimeric PSI of *psaF2*⁻ and *psaJ2*⁻ which both having the emission peak of PSI located at 743 nm and have 2 nm blue shift compared with the trimeric PSI of FRL Syn7335-WT.

4. Discussion

4.1 The blue shift of psaF2- and psaJ2- under RT and 77K fluorescence spectrum

In the fluorescence spectra, the psaF2 and psaJ2 have peaks slightly blue-shifted compared with the one in WT (fig. 13, fig. 14). And this result corresponds to previous research that simultaneously knockout white light type of psaF and psaJ in Synechocystis PCC 6803 (Jeanjean et al., 2003). The authors proposed that peaks slightly blue-shifted in fluorescence spectra may arise from the knockout of psaF and psaJ, causing the cells to express isiA and isiB, similar to iron-deficient stress. This possibility can be ruled out after conducting the MS/MS experiment to identify the protein in psaF2⁻ and psaJ2⁻. Here, the symptom can also be seen when knocking out far-red light type psaF2 or psaJ2, respectively. From this data, we can infer that losing PsaF2 or PsaJ2 would not affect the trimeric structure of PSI but may cause some stress with symptoms similar to irondeficient stress. The other possibility is that removing PsaF2 or PsaJ2 may cause the removal of A1 and A2 chlorophyll dimer (C. J. Gisriel et al., 2022), that the A1 and A2 chlorophyll dimer may originally contribute to much longer wavelength fluorescence emission. Also, the removal of PsaF2 and PsaJ2 may cause the Chl A38/A39 dimer to monomerize, which could originally offer the ability to absorb longer wavelength energy (C. J. Gisriel et al., 2022). Based on the structural analysis of cryo-EM, the blue shift happening in the absorbance and fluorescence spectrum when losing PsaF2 or PsaJ2 may result from losing the chlorophylls nearby, which may contribute to FRL absorbance or fluorescence emission.

4.2 The Chl f binding site specification near PsaJ2

In the HPLC analysis of the trimeric structure of *psaJ2*⁻, the number of Chl *f* molecules was lower compared with FRL Syn7335-WT and the *psaF2*⁻. And in the previous studies of cryo-EM, they found that the sequence homology of the PsaJ2 sidechain is the same as *Fischerella* 7521 and *Halomicronema hongdechloris*, which have the PsaJ2-Tyr sidechain to serve as H-bond to the Chl *f* B30 (C. J. Gisriel et al., 2022). Moreover, the sites B30 and B7 are related by the pseudo C2 symmetry toward the core; it was proposed to be one of the six high-specificity Chl *f* binding sites in FRL Syn7335 PSI (C. J. Gisriel et al., 2022). Combined with the structural studies, our mutagenesis results of HPLC analysis (**fig. 10**, **fig. 11**) can serve as another evidence that B30 in FRL-PSI is the Chl *f* binding site.

4.3 PSI structure changes in *psaI2*⁻ and *psaL2*⁻ and the exploration of Chl f binding abilities

In the absorption spectra and RT fluorescence spectra of the FRL psal2⁻ and psal2⁻ cells, the FRL absorbance ability, Chl f emission peak height of psal2⁻ and psal2⁻ and psal2⁻ were strongly decreased (fig. 7, fig. 8). And in the PSI isolation experiment results, the two mutants of psal2⁻ and psal2⁻ lost their trimeric structure of PSI. Also, these results can be compared with previous studies that knockout WL-type psal and psal and found that the trimeric structure of PSI is affected (Karapetyan et al., 1999; Schluchter et al., 1996). Furthermore, in the cryo-EM structure of FRL Syn7335-WT PSI structure, it proposed six high-specificity Chl f binding sites. The sites of B37 and B38 are very closely related to the region of Psal2, and B7 is closely related to Psal2 (Christopher J. Gisriel, David A. Flesher, et al., 2022; Christopher J. Gisriel, Gaozhong Shen, et al., 2022). Based on the structural data of cryo-EM (fig. 3), the decrease of FRL absorbance ability (fig. 7), Chl f emission peak height (fig. 8) of psal2⁻ and psal2⁻ can be attributed not only to the PSI structure and also to the decrease of Chl f molecules. The function of Psal2 and Psal2 may serve as the bridge to connect each PSI monomers and participate a vital character in the binding of Chl f molecules.

5. Conclusion and future works

To summarize the importance of the results, knockout psaI2 and psaL2 would strongly affect the growth of the Syn7335 cells under FRL. In contrast, knockout psaF2 and psaJ2 would not affect the Syn7335 cells' growth under WL or FRL. Further, psaL2 cells have lower FRL absorbance ability, and psal2 and psaL2 cells have lower Chl f emission peak height detected under RT fluorescence spectra. And for the PSI isolation result, psaF2⁻ and psaJ2 can still form the trimeric structure of PSI, whereas psaI2⁻ and psaL2 cannot form trimeric structures of PSI and only have one green band located on the upper layer of the sucrose gradient. In the absorption spectra, RT fluorescence spectra, and 77K fluorescence spectra of the trimeric PSI, trimeric PSI purified from psaF2⁻ and psaJ2⁻ have blue-shifted peaks of Chl a absorbance, Chl f emission peak, and emission peak of PSI compared with trimeric PSI purified form FRL Syn7335-WT. The blue-shifted phenomenon in psaF2 and psaJ2 may arise from the loss of PsaF2 and PsaJ2, respectively, or both of PsaF2 and PsaJ2, causing the symptom similar to iron deficient and express isiA and isiB. And the latter possibility can be ruled out in the future by sodium dodecyl sulfate polyacrylamide gel electrophoresis (SDS-PAGE) to identify protein subunits in psaF2⁻ and psaJ2⁻. Also, the trimeric PSI of psaF2⁻ and psaJ2⁻ can be sent to LC-MS/MS to identify the protein in psaF2⁻ and psaJ2⁻. And for the other possibility is that removing PsaF2 or PsaJ2 may cause loss of A1 and A2 chlorophyll dimer (C. J. Gisriel et al., 2022), which might contribute to much longer wavelength fluorescence emission. Also, the removal of PsaF2 and PsaJ2 may cause the Chl A38/A39 monomerization, which initially served the ability to absorb longer wavelength energy (C. J. Gisriel et al., 2022). This possibility can be further unraveled by sending the trimeric PSI purified from psaF2⁻ and psaJ2⁻ to identify the structure and chlorophyll molecules binding nearby under cryo-EM.

The decrease of FRL absorbance ability and Chl f emission peak height in psal2 and psal2 can be attributed to the PSI structure and reduced Chl f molecules. In summary, Psal2 and Psal2 can serve as bridges connecting three independent PSI monomers into PSI trimer and also participate in binding with Chl f molecules.

Figures



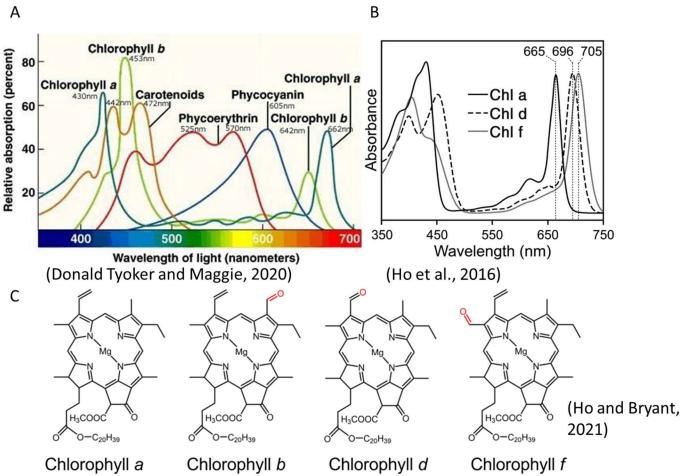
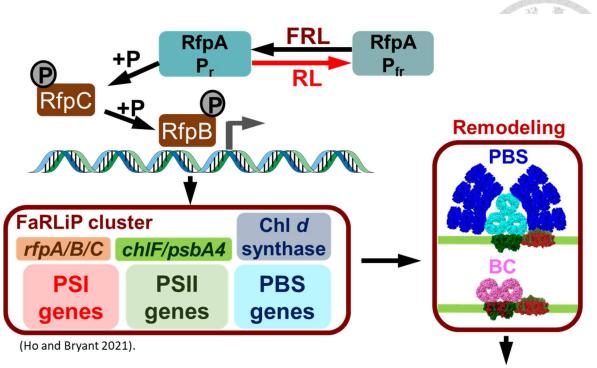


Fig. 1 Protein and pigments absorption spectra and the structure of chlorophylls

Fig. 1A is modified from (Donald Tyoker & Maggie, 2020); the central absorbance peak of chlorophyll a, chlorophyll b, and carotenoids is mainly located in the blue, purple, red, and orange regions. In contrast, phycoerythrin and phycocyanin have absorbance peaks in green and yellow areas. In **fig. 1B**, modified from (Ho et al., 2016), the absorbance peak of chlorophyll d and chlorophyll f is located at 696 nm and 705 nm, respectively, which is more closely to the far-red region compared with chlorophyll a with a center at 665 nm. The chemical structures of Chl a, Chl b, Chl d, and Chl f are shown in **fig. 1C** (modified from (Ho & Bryant, 2021)), and the different sites are marked with red.



Utilize FRL for photosynthesis and growth

Fig. 2 Regulation mechanism of FaRLiP.

Fig. 2 is modified from (Ho & Bryant, 2021). Receiving the light of FRL, the P_{fr} form of RfpA would turn into P_r form and then phosphorylate downstream RfpC. Further, the phosphorylated RfpC would phosphorylate RfpB, open the downstream FaRLiP gene cluster, and express 20 genes to remodel PSII, PSI, and phycobilisomes.

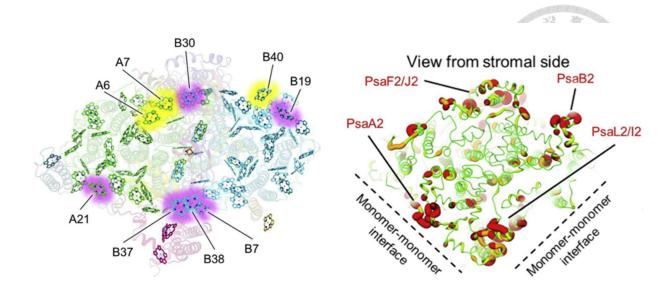


Fig. 3 Possible Chl f binding sites based on the cryogenic electron microscopy (cryo-EM) data from (C. J. Gisriel et al., 2022; C. J. Gisriel et al., 2020)

Fig. 3 is modified from (C. J. Gisriel et al., 2022). In the structural data identified under cryo-EM, several possible Chl *f* molecules binding sites were proposed based on visual inspection of the electrostatic potential map to the C2 moieties and cone scan analysis. The chlorophyll sites with a pink glow indicate the higher specificity of Chl *f* binding sites. In contrast, the chlorophyll sites with a yellow glow show the lower specificity Chl *f* binding sites. Here four subunits (*psaF2*, *psaJ2*, *psaJ2*, and *psaL2*) near the possible binding sites were chosen as the target gene for further mutagenesis study.

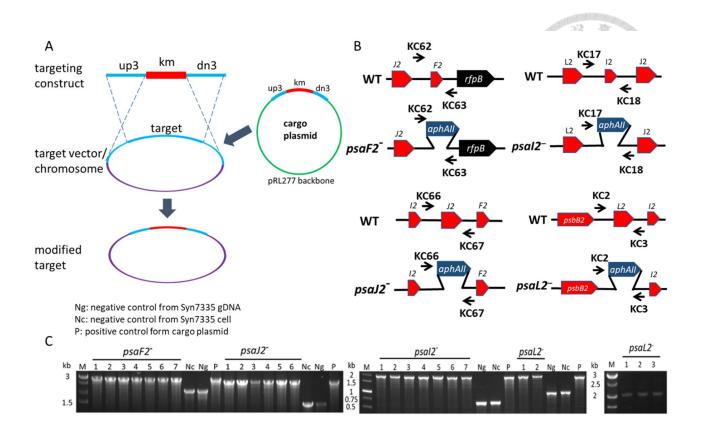


Fig. 4 Cargo plasmids are designed for conjugal transformation, and the colony PCR results of conjugation

Each cargo plasmid was carried with kanamycin-resistant cassette *aphAII* and flanked with two 3 kb segments PCR amplified from the target genes as shown in **fig. 4A**. They were further transformed into *E. coli* strain HB101 supplemented with conjugal plasmid pRL443 and helper plasmids pRL623. In **fig. 4A**, the E. coli was used for further conjugal transformation into Syn7335. After the conjugal transformation, the colonies of the mutants (*psaF2*-, *psaI2*-, *psaJ2*-, and *psaL2*-) were further examined by colony PCR with the primers shown in **fig. 4B**. The colony PCR results of the conjugants are shown in **fig. 4C**.

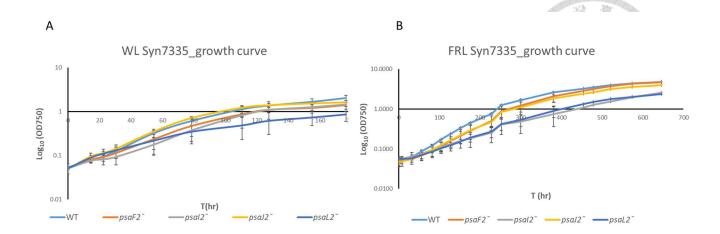


Fig. 5 Growth curve of Syn7335 WT and mutants under WL and FRL.

The WT and mutants' (*psaF2*-, *psaJ2*-, *psaJ2*-, and *psaL2*-) growth curves of Syn7335 were grown under a light intensity of 100 μmol photons m⁻² s⁻¹ visible light and far-red light (LED centered at 730 nm) of light intensity of 100 μmol photons m⁻² s⁻¹. In **Fig. 5A**, Syn7335-WT and the mutants (*psaF2*-, *psaJ2*-, *psaJ2*-, and *psaL2*-) growth curves are similar when grown under WL. Whereas, in FRL (**fig. 5B**), *psaI2*- and *psaL2*- grew slower compared with Syn7335-WT, *psaF2*-, and *psaJ2*-.



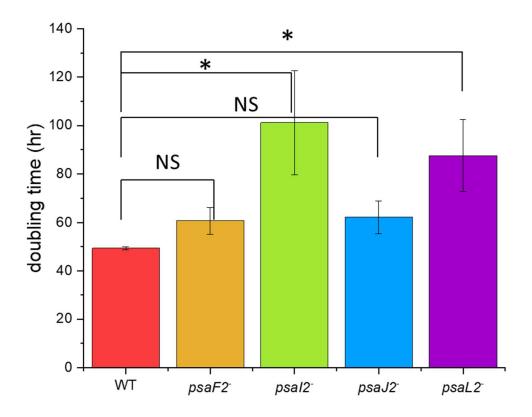


Fig. 6 The doubling time of the FRL Syn7335-WT and the four mutants (*psaF2*-, *psaI2*-, *psaJ2*-, and *psaL2*-) cells.

(https://www.statskingdom.com/kruskal-wallis-calculator.html)

The p-value was calculated with the Kruskal-Wallis calculator with a significance level: *p<0.05; NS: no significant difference. In **fig. 6**, the doubling time of Syn7335-WT has the lowest doubling time when grown under FRL but has no significant difference between $psaF2^-$ and $psaJ2^-$. However, the doubling time of $psaI2^-$ and $psaJ2^-$ have significantly longer doubling times compared with Syn7335-WT under FRL.

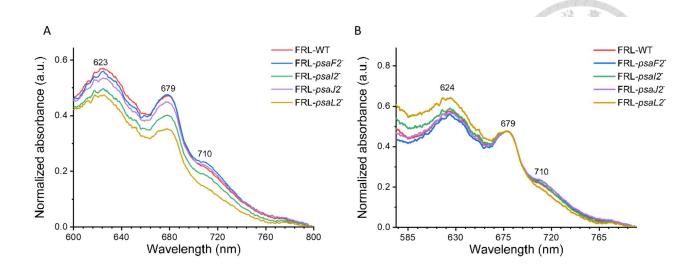


Fig. 7 Syn7335 WT and mutants' (psaF2-, psaI2-, psaJ2-, and psaL2-) absorption spectra

In the absorption spectra (**fig. 7A**), the FRL absorbance peak (700 – 750 nm) of *psa12*and *psaL2*- was lower than others. And in **fig. 7B**, the absorption curves were normalized
at the picked point at 680 nm. The *psaF2*- and *psaJ2*- cells have the highest FRL
absorption peak height, FRL Syn7335-WT, *psa12*- cells ranked second, and *psaL2*- has
the lowest FRL absorbance ability.

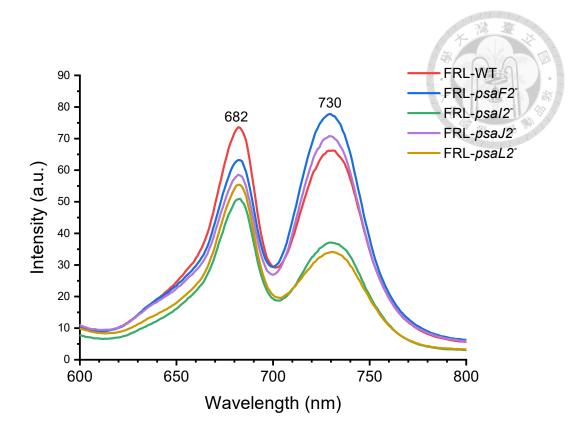


Fig. 8 The RT fluorescence spectrum of the FRL Syn7335-WT and the four mutants (psaF2-, psaI2-, psaI2-, psaI2-) cells

As shown in **fig. 8**, $psaF2^-$ and $psaJ2^-$ have the highest Chl f emission peak at around 730 nm, slightly higher than the Chl f emission peak of FRL Syn7335-WT. Otherwise, $psaI2^-$ and $psaL2^-$ have the lowest Chl f emission peak height at around 730 nm.



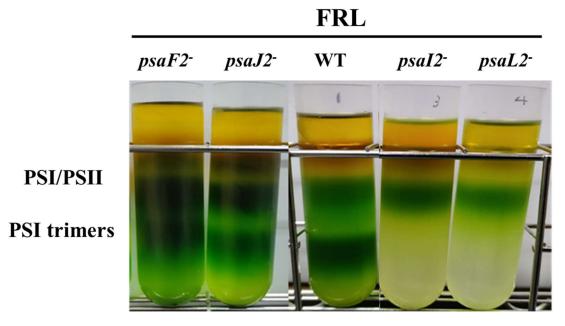


Fig. 9 Isolation of PSI complexes from Syn7335-WT and *psaF2*-, *psaI2*-, *psaI2*-, *psaI2*-, *psaL2*- cells

In **fig. 9**, the monomeric and trimeric fractions containing PSI and PSII were isolated by ultracentrifugation. In the isolated result, the trimeric structure of PSI can only be found in FRL-WT, *psaF2*⁻, and *psaJ2*⁻ but cannot be found in FRL *psaI2*⁻ and *psaL2*⁻.

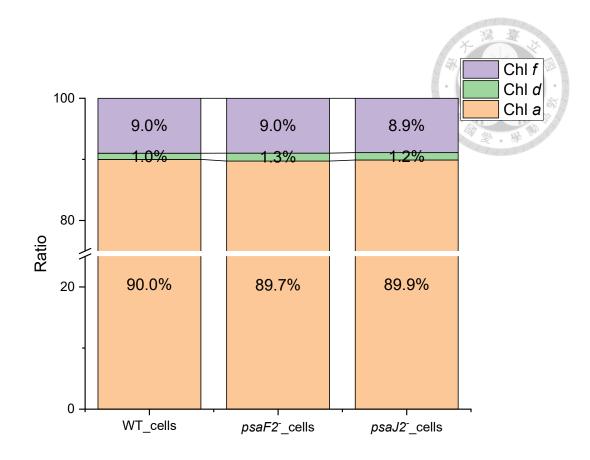


Fig. 10 The chlorophyll ratio of Chl a: Chl d: Chl f in the 100 % stacked bar chart of FRL Syn7335-WT, psaF2⁻, psaJ2⁻ cells

The Chl f ratios do not change much along with psaF2-, psaJ2-, and WT in cells. Here the Chl d molecules were produced when extracted the pigments since the Chl a molecules would spontaneously turn into Chl d molecules non-enzymatically (Fukusumi et al., 2012).

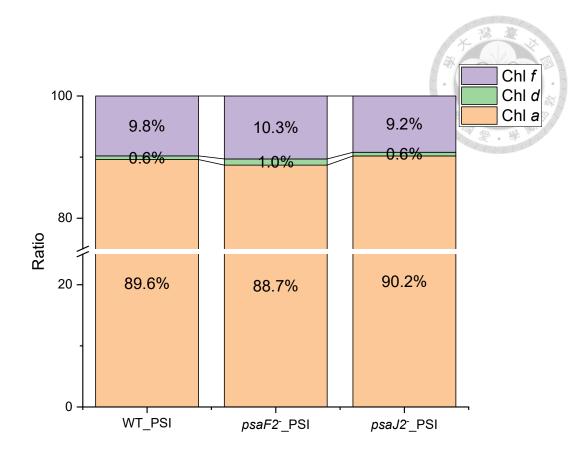


Fig. 11 The chlorophyll ratio of Chl a: Chl d: Chl f in the 100 % stacked bar chart of the trimeric PSI purified from FRL Syn7335-WT, psaF2-, psaJ2-

In **fig. 11** shows lower chlorophyll f in the $psaJ2^-$ PSI trimer compared with the trimeric PSI purified from FRL Syn7335-WT and $psaF2^-$. Here the Chl d molecules were produced when extracted the pigments since the Chl a molecules would spontaneously turn into Chl d molecules non-enzymatically (Fukusumi et al., 2012).

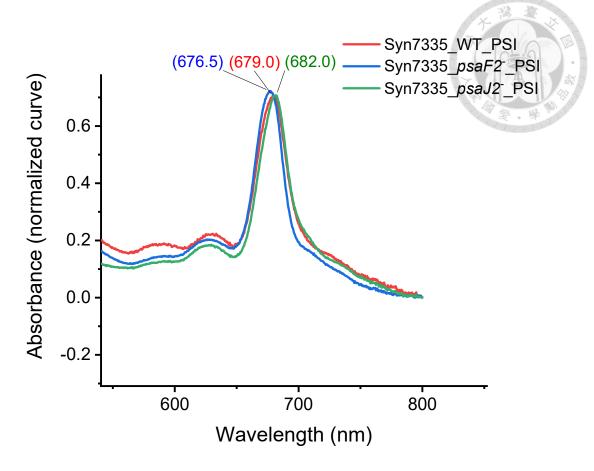


Fig. 12 Absorbance spectra of Syn7335 WT, psaF2⁻, psaJ2⁻ PSI trimer.

The absorbance spectra curves of the trimeric PSI purified from FRL Syn7335-WT, $psaF2^-$, and $psaJ2^-$ are shown in **fig. 12**. The absorbance spectra shown in **fig. 12** are normalized from 0-1 and then normalized to the peak point at 680 nm. In the absorbance spectra, the PSI trimer of psaF2 has slightly blue shift peaks at around 680 nm compared with the PSI trimer of FRL Syn7335-WT.

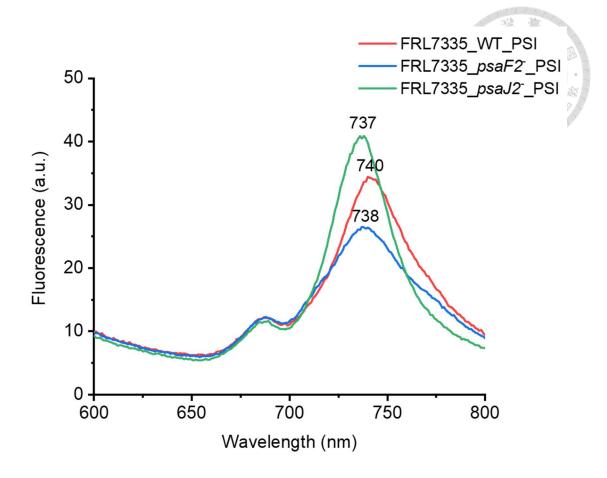


Fig. 13 RT fluorescence spectra of Syn7335 WT, psaF2-, psaJ2- PSI trimer.

In **fig. 13**, the PSI trimer of *psaF2*⁻ has the lowest Chl *f* emission peak height compared with the PSI trimer of FRL Syn7335-WT and *psaJ2*⁻. Also, the Chl *f* emission peak of *psaF2*⁻ and *psaJ2*⁻ slightly blue shift to 738 nm and 737 nm, respectively, which is different from the Chl *f* emission peak of the FRL Syn7335-WT PSI trimer located at 740 nm.

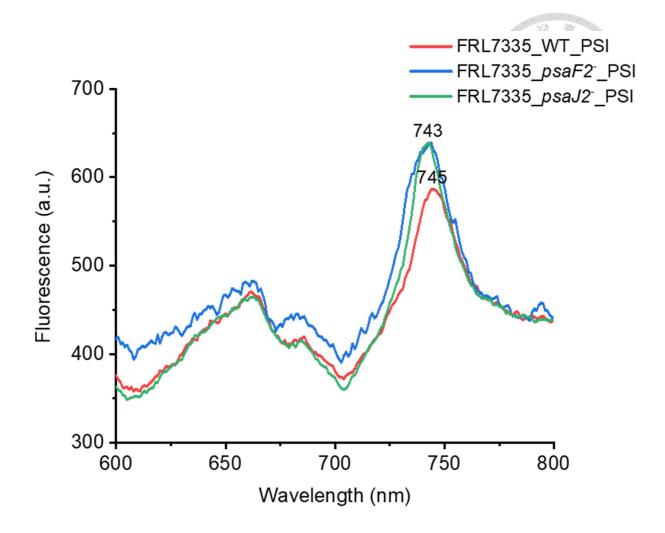


Fig. 14 77K fluorescence spectrum of Syn7335 WT, psaF2⁻, psaJ2⁻ PSI trimer.

In **fig. 14**, the PSI trimer of *psaF2*⁻ and *psaJ2*⁻ have a blue shift of the PSI emission peak located at 743 nm, which has a two nanometers shift compared with the PSI emission peak of FRL Syn7335-WT PSI located at 745 nm.

Tables

Table 1 Medium solution of ASN-III liquid and plate

ASNIII liquid medium & 1.75% plate

| | 1L |
|---|--|
| NaCl | 25.0 g |
| MgSO ₄ ·7H ₂ O | 3.5 g |
| MgCl ₂ ·6H ₂ O | 2.0 g |
| NaNO ₃ | 0.75 g |
| CaCl ₂ ·2H ₂ O | 0.5 g |
| KCl | 0.5 g |
| Na ₂ CO ₃ | 0.02 g |
| Citric acid | 1 ml from stock (3.0 mg) |
| Ferric ammonium citrate | 1 ml from stock (3.0 mg) |
| A-5 trace minerals | 1.0 ml |
| EDTA | 0.167 ml from 3g/L stock (0.5 mg) |
| Vitamin B ₁₂ (Add after autoclave) | 1 ml from stock (4.0 mg) |
| K ₂ HPO ₄ (Add after autoclave) | 1 ml from stock (0.064 g) |
| 1 M Tris-HCl, pH 8 (Add after autoclave) | 10 ml |
| Triple-washed Bacto agar | 17.5 g |
| Distilled water to | 1.0 L |

Final pH ~8.6 at room temperature

Trace metal mix A5:

| H ₃ BO ₃ | 2.86 g |
|--|---------|
| MnCl ₂ ·4H ₂ O | 1.81 g |
| ZnSO ₄ ·7H ₂ O | 0.222 g |
| Na ₂ MoO ₄ ·2H ₂ O | 0.39 g |
| CuSO ₄ ·5H ₂ O | 0.079 g |
| Co(NO ₃) ₂ ·6H ₂ O | 49.4 mg |
| Distilled water | 1.0 L |



Table 2 Primers used in this study

| primer name | Size (base) | Sequence (5' to 3') | description |
|-----------------------|-------------|-----------------------|---|
| (KC1)-7335-pasL2-3kb- | 60 | TTCGCCCAGCTTCTGTATGGA | for amplification of the 3 kb |
| upstream-F | | ACGGGCATGGGAAAATGCAG | upstream region of <i>psaL2</i> in |
| | | TCAGATGTCTGGGGAGCGG | Syn7335 |
| (KC2)-7335-pasL2-3kb- | 59 | CCTTGCGCCCTGAGTGCTTGC | for amplification of the 3 kb |
| upstream-R | | GGCAGCGTGGGATCCAGAAA | upstream region of <i>psaL2</i> in |
| | | TAACCTCACTAGAATTGC | Syn7335 |
| (KC3)-7335-pasL2-3kb- | 59 | ATCTCATGCTGGAGTTCTTCG | for amplification of the 3 kb |
| downstream-F | | CCCACCACTAGTTTTTGTTCT | downstream region of <i>psaL2</i> |
| | | TCTTTTGTTCTTCATAG | in Syn7335 |
| (KC4)-7335-pasL2-3kb- | 60 | CGCAACGTTGTTGCCATTGCT | for amplification of the 3 kb |
| downstream-R | | GCAGGCATGGCCTATCTAGCT | downstream region of <i>psaL2</i> |
| | | GGCTCGATCTCAAGTCTC | in Syn7335 |
| (KC5)- | 22 | AGAGTACTGCTGGGGCAAGC | colony PCR primer for conjugated |
| pasL2_km_seqencing_F | | CA | |
| (KC6)- | 24 | GGCGATCGCGAATATTGGGAA | colony PCR primer for |
| pasL2_km_seqencing_R | | GGG | conjugated plasmid pRL277- 7335-psaL2-Km |
| (KC7)- | 22 | CGACTCACCCCGTCGCCTATG | sequencing primer for |
| pRL277_7335psaL2Km_se | | A | conjugated plasmid 7335- |
| q_F1 | | | pRL277 <i>-psaL2</i> -km |
| (KC8)- | 22 | AGGGAACTGGGGAGCCTATG | sequencing primer for |
| pRL277_7335psaL2Km_se | | CG | conjugated plasmid 7335- |
| q_F2 | | | pRL277 <i>-psaL2</i> -km |
| | | | • |

| (KC9)- | 25 | GCTCTCTATGGCATTAGCTCG | sequencing primer for |
|-------------------------|----|-----------------------|-------------------------------|
| pRL277_7335psaL2Km_se | | CTGC | conjugated plasmid 7335- |
| q_F3 | | | pRL277-psaL2-km |
| (KC10)- | 22 | TACTGGCAGCAGGTTCCCGT | sequencing primer for |
| pRL277_7335psaL2Km_se | | GA | conjugated plasmid 7335- |
| q_F4 | | | pRL277 <i>-psaL2</i> -km |
| (KC11)- | 22 | CTGCTCTGATGCCGCCGTGTT | sequencing primer for |
| pRL277_7335psaL2Km_se | | С | conjugated plasmid 7335- |
| q_F5 | | | pRL277 <i>-psaL2</i> -km |
| (KC12)- | 22 | TTTCGATTCCACCGCCGCCTT | sequencing primer for |
| pRL277_7335psaL2Km_se | | С | conjugated plasmid 7335- |
| q_F6 | | | pRL277 <i>-psaL2</i> -km |
| (KC13)- | 22 | GCTAACTTGCTTTGCGGCGCA | sequencing primer for |
| pRL277_7335psaL2Km_se | | G | conjugated plasmid 7335- |
| q_F7 | | | pRL277 <i>-psaL2</i> -km |
| (KC14)- | 22 | CCTGCTCTTGAACGCCGCTCT | sequencing primer for |
| pRL277_7335psaL2Km_se | | Т | conjugated plasmid 7335- |
| q_F8 | | | pRL277-psaL2-km |
| (KC15)- | 22 | TGAAAGGGCTGCGTCGAAAG | sequencing primer for |
| pRL277_7335psaL2Km_se | | CT | conjugated plasmid 7335- |
| q_F9 | | | pRL277 <i>-psaL2</i> -km |
| (KC16)-7335-pRL277- | 59 | TCGCCCAGCTTCTGTATGGAA | for amplification of the 3 kb |
| psaI2-km-3kb-upstream-F | | CGGGCATGGCGTCCCATTTTG | upstream region of psaI2 in |
| | | GCCATCTTGCCATTATC | Syn7335 |
| (KC17)-7335-pRL277- | 59 | CCCTGAGTGCTTGCGGCAGC | for amplification of the 3 kb |
| psaI2-km-3kb-upstream-R | | GTGGGATCCCTCATCAAATCT | upstream region of psaI2 in |

| | | CCTATCCAATCGTAAGGG | Syn7335 |
|---|----|---|--|
| (KC18)-7335-pRL277- | 59 | CATGCTGGAGTTCTTCGCCCA | for amplification of the 3 kb |
| psaI2-km-3kb- | | CCACTAGTCGACTCAACCGC | downstream region of psaI2 |
| downstream-F | | AACTTGATATTCCGTGTC | in Syn7335 |
| (KC19)-7335-pRL277- | 59 | GCAACGTTGTTGCCATTGCTG | for amplification of the 3 kb |
| psaI2-km-3kb- | | CAGGCATGGCGGCATCGAGA | downstream region of psaI2 |
| downstream-R | | TATCTAATAGCAGCAAAT | in Syn7335 |
| (KC20)-7335-pRL277- | 40 | TTCTGTATGGAACGGGCATGG | for amplification of the 3 kb |
| psaI2-km-3kb-upstream-F- | | CGTCCCATTTTGGCCATCT | upstream region of psaI2 in |
| automatic_generate | | | Syn7335 |
| (KC21)-7335-pRL277- | 44 | CTTGCGGCAGCGTGGGATCC | for amplification of the 3 kb |
| psaI2-km-3kb-upstream-R- | | CTCATCAAATCTCCTATCCAAT | upstream region of psaI2 in |
| automatic_generate | | CG | Syn7335 |
| (KC22)-7335-pRL277- psaI2-km-3kb- downstream-F- automatic generate | 40 | GTTCTTCGCCCACCACTAGTC GACTCAACCGCAACTTGAT | for amplification of the 3 kb downstream region of <i>psal2</i> in Syn7335 |
| (KC23)-7335-pRL277- psaI2-km-3kb- downstream-R- automatic_generate | 40 | TTGCCATTGCTGCAGGCATGG CGGCATCGAGATATCTAAT | for amplification of the 3 kb downstream region of <i>psaI2</i> in Syn7335 |
| (KC24)-7335-pRL277- psaI2- km_km_sequencing_F | 22 | TTGATGGGCTCATTAGGCGGC G | colony PCR primer for conjugated plasmid pRL277- 7335-psal2-Km |

| (KC25)-7335-pRL277- | 22 | CGGTGAGGAAGCGCAGGGA | colony PCR primer for |
|------------------------|----|-----------------------|----------------------------|
| psaI2- | | ACT | conjugated plasmid pRL277- |
| km_km_sequencing_R | | | 7335 <i>-psaI2</i> -Km |
| (KC26)-7335-pRL277- | 22 | TTGATGGGCTCATTAGGCGGC | colony PCR primer for |
| psaI2- | | G | conjugated plasmid pRL277- |
| km_colony_PCR_primer_F | | | 7335 <i>-psaI2</i> -Km |
| (KC27)-7335-pRL277- | 22 | CGGTGAGGAAGCGCAGGGA | |
| psaI2- | | ACT | colony PCR primer for |
| km_colony_PCR_primer_ | | | conjugated plasmid pRL277- |
| R | | | 7335 <i>-psaI2</i> -Km |
| (KC28)- | 22 | ATTCCTGAATCGCGCGGACA | sequencing primer for |
| pRL277_7335psaI2Km_se | | GC | conjugated plasmid 7335- |
| q_F2 | | | pRL277 <i>-psaI2</i> -km |
| (KC29)- | 22 | CGCCTTTGGTAGCCCGGACA | sequencing primer for |
| pRL277_7335psaI2Km_se | | AA | conjugated plasmid 7335- |
| q_F3 | | | pRL277-psaI2-km |
| (KC30)- | 22 | CTATCGATTGTGCAGGCGCGG | sequencing primer for |
| pRL277_7335psaI2Km_se | | Т | conjugated plasmid 7335- |
| q_F4 | | | pRL277-psaI2-km |
| (KC31)- | 22 | CGACTGCGTCCGCTCCGTAA | sequencing primer for |
| pRL277_7335psaI2Km_se | | AA | conjugated plasmid 7335- |
| q_F5 | | | pRL277-psaI2-km |
| (KC32)- | 22 | GGGCGCCCGGTTCTTTTTGTC | sequencing primer for |
| pRL277_7335psaI2Km_se | | A | conjugated plasmid 7335- |
| q_F6 | | | pRL277-psa12-km |
| (KC33)- | 22 | TTTCGATTCCACCGCCGCCTT | sequencing primer for |

| pRL277_7335psaI2Km_se | | С | conjugated plasmid 7335- |
|-----------------------|----|------------------------|------------------------------------|
| q_F7 | | | pRL277- <i>psaI2</i> -km |
| (KC34)- | 22 | TCGACCACCTCTACCGTGACC | sequencing primer for |
| pRL277_7335psaI2Km_se | | A | conjugated plasmid 7335- |
| q_F8 | | | pRL277-psaI2-km |
| (KC35)- | 23 | TGTCAGCAACTACGTGCCCA | sequencing primer for |
| pRL277_7335psaI2Km_se | | AGA | conjugated plasmid 7335- |
| q_F9 | | | pRL277 <i>-psaI2</i> -km |
| (KC36)- | 22 | CGCACAGTTTGACAGGGGTG | sequencing primer for |
| pRL277_7335psaI2Km_se | | CT | conjugated plasmid 7335- |
| q_F10 | | | pRL277 <i>-psaI2</i> -km |
| (KC61)-7335-psaF2- | 59 | TCGCCCAGCTTCTGTATGGAA | for amplification of the 3 kb |
| upstream-3kb-F | | CGGGCATGGGCTGCATTTGCA | upstream region of <i>psaF2</i> in |
| | | ACCGCGATATCGGCCTA | Syn7335 |
| (KC62)-7335-psaF2- | 59 | GAGTGCTTGCGGCAGCGTGG | for amplification of the 3 kb |
| upstream-3kb-R | | GATCCAGCTATGTTTTCCTAAT | upstream region of psaF2 in |
| | | AAACGAATAAATCTTGG | Syn7335 |
| (KC63)-7335-psaF2- | 59 | CATGCTGGAGTTCTTCGCCCA | for amplification of the 3 kb |
| downstream-3kb-F | | CCACTAGTCAGCCATCTCGAC | downstream region of psaF2 |
| | | CACCTCTACCGTGACCA | in Syn7335 |
| (KC64)-7335-psaF2- | 59 | GCAACGTTGTTGCCATTGCTG | for amplification of the 3 kb |
| downstream-3kb-R | | CAGGCATGCAGTGCAACTT | downstream region of psaF2 |
| | | TAGCTTCACTGCTTAACA | in Syn7335 |
| (KC65)-7335-psaJ2- | 59 | TCGCCCAGCTTCTGTATGGAA | for amplification of the 3 kb |
| upstream-3kb-F | | CGGGCATGGTTAGGCTGGCA | upstream region of psaJ2 in |
| | | CCTAGCCTGCCTTGGTGT | Syn7335 |

| (KC66)-7335-psaJ2- | 59 | CCCTGAGTGCTTGCGGCAGC | for amplification of the 3 kb |
|------------------------|----|-----------------------|-----------------------------------|
| upstream-3kb-R | | GTGGGATCCGTGGGTTCTCCA | upstream region of psaJ2 in |
| | | GACAGTAGAGTTGGTCAC | Syn7335 |
| (KC67)-7335-psaJ2- | 59 | CATGCTGGAGTTCTTCGCCCA | for amplification of the 3 kb |
| downstream-3kb-F | | CCACTAGTGCTAGCCCAAAG | downstream region of psaJ2 |
| | | TCGTATCAATAGCTACGA | in Syn7335 |
| (KC68)-7335-psaJ2- | 59 | GCAACGTTGTTGCCATTGCTG | for amplification of the 3 kb |
| downstream-3kb-R | | CAGGCATGGCTGGACAATCT | downstream region of <i>psaJ2</i> |
| | | CTAGCTCCCGATCACCAA | in Syn7335 |
| (KC105)-7335-pRL277- | 22 | TCTGGGACCCTCAGTTTGGG | sequencing primer of 7335- |
| psaL2-km-mut_seq_p | | CC | pRL277-psaL2-km |
| | | | conjugants |
| (KC106)-pRL277-colony- | 22 | CTACACGACGGGGAGTCAGG | colony PCR primer to ensure |
| PCR-primer-set1-F | | CA | backbone is not inserted into |
| | | | Syn7335 |
| (KC107)-pRL277-colony- | 22 | ACGTGCAGCTTTCCCTTCAGG | colony PCR primer to ensure |
| PCR-primer-set1-R | | С | backbone is not inserted into |
| | | | Syn7335 |
| (KC108)-pRL277-colony- | 23 | CCCGCGCGATTTACTTTTCGA | colony PCR primer to ensure |
| PCR-primer-set2-F | | CC | backbone is not inserted into |
| | | | Syn7335 |
| (KC109)-pRL277-colony- | 22 | ACGTGCAGCTTTCCCTTCAGG | colony PCR primer to ensure |
| PCR-primer-set2-R | | С | backbone is not inserted into |
| | | | Syn7335 |
| (KC110)-7335-pRL277- | 22 | AATCCTGTCCAGCCTGGGCCT | sequencing primer of 7335- |
| psaL2-km-mut_seq_p_R | | Т | pRL277-psaL2-km |

| | | | conjugants |
|------------------------|----|-----------------------|------------------------------|
| (KC113)-7335-psaF2- | 22 | GGCTCATTAGGCGGCGCAATC | colony PCR primer for |
| colony-PCR-set1-F | | Т | conjugated plasmid pRL277- |
| | | | 7335 <i>-psaF2</i> -Km |
| (KC114)-7335-psaF2/J2- | 22 | GCAGTCCTTCCCACTCGAGG | colony PCR primer for |
| colony-PCR-set1-R | | GT | conjugated plasmid pRL277- |
| | | | 7335 <i>-psaF2/psaJ2</i> -Km |
| (KC115)-7335-psaJ2- | 22 | GCCTGCTGTTGCTGCCTCAGA | colony PCR primer for |
| colony-PCR-set1-F | | A | conjugated plasmid pRL277- |
| | | | 7335 <i>-psaJ2</i> -Km |
| (KC116)-pRL277-7335- | 22 | TGGCGCATCACCATTTGGCGA | sequencing primer for |
| psaF2_km_seq_F1 | | T | conjugated plasmid 7335- |
| | | | pRL277 <i>-psaF2</i> -km |
| (KC117)-pRL277-7335- | 22 | TGCGATCGCACTTGGTCTACA | sequencing primer for |
| psaF2_km_seq_F2 | | TGT | conjugated plasmid 7335- |
| | | | pRL277-psaF2-km |
| (KC118)-pRL277-7335- | 22 | ACAAACTTTCTTTGCGATCGC | sequencing primer for |
| psaF2_km_seq_F3 | | T | conjugated plasmid 7335- |
| | | | pRL277 <i>-psaF2</i> -km |
| (KC119)-pRL277-7335- | 22 | TCTGCCCTTCCCAATATTCGC | sequencing primer for |
| psaF2_km_seq_F4 | | GA | conjugated plasmid 7335- |
| | | | pRL277-psaF2-km |
| (KC120)-pRL277-7335- | 22 | CCTGAATGAACTGCAGGACG | sequencing primer for |
| psaF2_km_seq_F5 | | AGGC | conjugated plasmid 7335- |
| | | | pRL277-psaF2-km |
| (KC121)-pRL277-7335- | 22 | TCGACCACCTCTACCGTGACC | sequencing primer for |

| psaF2_km_seq_F6 | | A | conjugated plasmid 7335- pRL277-psaF2-km |
|----------------------|----|-----------------------|---|
| (KC122)-pRL277-7335- | 22 | ACACCTTGCCTGTGCTTTTCG | sequencing primer for |
| psaF2_km_seq_F7 | | Т | conjugated plasmid 7335- |
| | | | pRL277 <i>-psaF2</i> -km |
| (KC123)-pRL277-7335- | 22 | GACGATCAGGCCCGCTTGGA | sequencing primer for |
| psaF2_km_seq_F8 | | TG | conjugated plasmid 7335- |
| | | | pRL277 <i>-psaF2</i> -km |
| (KC124)-pRL277-7335- | 22 | TGTCAAACGGTGCGTCGGTC | sequencing primer for |
| psaF2_km_seq_F9 | | AC | conjugated plasmid 7335- |
| | | | pRL277-psaF2-km |
| (KC125)-pRL277-7335- | 22 | CGCCTTTGGTAGCCCGGACA | sequencing primer for |
| psaJ2_km_seq_F1 | | AA | conjugated plasmid 7335- |
| | | | pRL277 <i>-psaJ2</i> -km |
| (KC126)-pRL277-7335- | 22 | GGTTGGTGGGCCTGGTTCAC | sequencing primer for |
| psaJ2_km_seq_F2 | | TT | conjugated plasmid 7335- |
| | | | pRL277 <i>-psaJ2</i> -km |
| (KC127)-pRL277-7335- | 22 | CGATAGCATTCTTCGAGGCGC | sequencing primer for |
| psaJ2_km_seq_F3 | | TGT | conjugated plasmid 7335- |
| | | | pRL277 <i>-psaJ2</i> -km |
| (KC128)-pRL277-7335- | 22 | GCTGGTCTGGCCGGGCTTATC | sequencing primer for |
| psaJ2_km_seq_F4 | | Т | conjugated plasmid 7335- |
| | | | pRL277 <i>-psaJ2</i> -km |
| (KC129)-pRL277-7335- | 22 | CCTGAATGAACTGCAGGACG | sequencing primer for |
| psaJ2_km_seq_F5 | | AGGC | conjugated plasmid 7335- |
| | | | pRL277 <i>-psaJ2</i> -km |

| (KC130)-pRL277-7335- | 22 | CGAGAAGGCTTACCGCTGGC | sequencing primer for |
|----------------------|----|-----------------------|--------------------------|
| psaJ2_km_seq_F6 | | TG | conjugated plasmid 7335- |
| | | | pRL277-psaJ2-km |
| (KC131)-pRL277-7335- | 22 | GGGAAGGACTGCGGCTAGAG | sequencing primer for |
| psaJ2_km_seq_F7 | | GT | conjugated plasmid 7335- |
| | | | pRL277 <i>-psaJ2</i> -km |
| (KC132)-pRL277-7335- | 22 | AGAGTCTTTGGTAGCGATGCT | sequencing primer for |
| psaJ2_km_seq_F8 | | A | conjugated plasmid 7335- |
| | | | pRL277 <i>-psaJ2</i> -km |
| (KC133)-pRL277-7335- | 22 | CGCCACCGCTAATAGCCCTAC | sequencing primer for |
| psaJ2_km_seq_F9 | | С | conjugated plasmid 7335- |
| | | | pRL277 <i>-psaJ2</i> -km |

References

- Chen, M., Quinnell, R. G., & Larkum, A. W. D. (2002). Chlorophyll d as the major photopigment in Acaryochloris marina. *Journal of Porphyrins and Phthalocyanines*, 06(12), 763-773.
 - https://doi.org/10.1142/s1088424602000889
- Donald Tyoker, K., & Maggie, C. (2020). Microalgae: The Multifaceted Biomass of the 21st Century. In B. Thalita Peixoto, B. Thiago Olitta, & B. Luiz Carlos (Eds.), *Biotechnological Applications of Biomass*. IntechOpen. https://doi.org/10.5772/intechopen.94090
- Elhai, J., Vepritskiy, A., Muro-Pastor, A. M., Flores, E., & Wolk, C. P. (1997). Reduction of conjugal transfer efficiency by three restriction activities of Anabaena sp. strain PCC 7120. *Journal of Bacteriology*, *179*(6), 1998-2005. https://doi.org/doi:10.1128/jb.179.6.1998-2005.1997
- Elhai, J., & Wolk, C. P. (1988). [83] Conjugal transfer of DNA to cyanobacteria. In *Methods in Enzymology* (Vol. 167, pp. 747-754). Academic Press. https://doi.org/https://doi.org/10.1016/0076-6879(88)67086-8
- Fukusumi, T., Matsuda, K., Mizoguchi, T., Miyatake, T., Ito, S., Ikeda, T., Tamiaki, H., & Oba, T. (2012). Non-enzymatic conversion of chlorophyll-a into chlorophyll-d in vitro: A model oxidation pathway for chlorophyll-d biosynthesis. *FEBS Letters*, *586*(16), 2338-2341.
 - https://doi.org/https://doi.org/10.1016/j.febslet.2012.05.036
- Gan, F., & Bryant, D. A. (2015). Adaptive and acclimative responses of cyanobacteria to far-red light. *Environ Microbiol*, *17*(10), 3450-3465. https://doi.org/10.1111/1462-2920.12992
- Gan, F., Zhang, S., Rockwell, N. C., Martin, S. S., Lagarias, J. C., & Bryant, D. A. (2014). Extensive remodeling of a cyanobacterial photosynthetic apparatus in far-red light. *Science*, 345(6202), 1312-1317. https://doi.org/10.1126/science.1256963
- Gisriel, C., Shen, G., Kurashov, V., Ho, M.-Y., Zhang, S., Williams, D., Golbeck, J. H., Fromme, P., & Bryant, D. A. (2020). The structure of Photosystem I acclimated to far-red light illuminates an ecologically important acclimation process in photosynthesis. *Science Advances*, *6*(6), eaay6415. https://doi.org/doi:10.1126/sciadv.aay6415
- Gisriel, C., Shen, G. Z., Kurashov, V., Ho, M. Y., Zhang, S. J., Williams, D., Golbeck, J. H., Fromme, P., & Bryant, D. A. (2020). The structure of Photosystem I acclimated to far-red light illuminates an ecologically important acclimation process in photosynthesis. *Science Advances*, 6(6), Article eaay6415.

https://doi.org/10.1126/sciadv.aay6415

- Gisriel, C. J., Flesher, D. A., Shen, G., Wang, J., Ho, M.-Y., Brudvig, G. W., & Bryant, D. A. (2022). Structure of a photosystem I-ferredoxin complex from a marine cyanobacterium provides insights into far-red light photoacclimation. *Journal of Biological Chemistry*, 298(1). https://doi.org/10.1016/j.jbc.2021.101408
- Gisriel, C. J., Flesher, D. A., Shen, G., Wang, J., Ho, M. Y., Brudvig, G. W., & Bryant, D. A. (2022). Structure of a photosystem I-ferredoxin complex from a marine cyanobacterium provides insights into far-red light photoacclimation. *J Biol Chem*, 298(1), 101408. https://doi.org/10.1016/j.jbc.2021.101408
- Gisriel, C. J., Huang, H.-L., Reiss, K. M., Flesher, D. A., Batista, V. S., Bryant, D. A., Brudvig, G. W., & Wang, J. (2021). Quantitative assessment of chlorophyll types in cryo-EM maps of photosystem I acclimated to far-red light. *BBA Advances*, *1*, 100019.
 - https://doi.org/https://doi.org/10.1016/j.bbadva.2021.100019
- Gisriel, C. J., Shen, G., Ho, M.-Y., Kurashov, V., Flesher, D. A., Wang, J., Armstrong, W. H., Golbeck, J. H., Gunner, M. R., Vinyard, D. J., Debus, R. J., Brudvig, G. W., & Bryant, D. A. (2022). Structure of a monomeric photosystem II core complex from a cyanobacterium acclimated to far-red light reveals the functions of chlorophylls d and f. *Journal of Biological Chemistry*, 298(1), 101424. https://doi.org/https://doi.org/10.1016/j.jbc.2021.101424
- Gisriel, C. J., Wang, J., Brudvig, G. W., & Bryant, D. A. (2020). Opportunities and challenges for assigning cofactors in cryo-EM density maps of chlorophyll-containing proteins. *Communications Biology*, *3*(1), 408. https://doi.org/10.1038/s42003-020-01139-1
- Ho, M.-Y., & Bryant, D. A. (2021). Photosynthesis | Long Wavelength Pigments in Photosynthesis. In J. Jez (Ed.), *Encyclopedia of Biological Chemistry III (Third Edition)* (pp. 245-255). Elsevier. https://doi.org/https://doi.org/10.1016/B978-0-12-819460-7.00009-8
- Ho, M.-Y., Gan, F., Shen, G., Zhao, C., & Bryant, D. A. (2017). Far-red light photoacclimation (FaRLiP) in Synechococcus sp. PCC 7335: I. Regulation of FaRLiP gene expression. *Photosynthesis Research*, 131(2), 173-186. https://doi.org/10.1007/s11120-016-0309-z
- Ho, M.-Y., Shen, G., Canniffe, D. P., Zhao, C., & Bryant, D. A. (2016). Light-dependent chlorophyll f synthase is a highly divergent paralog of PsbA of photosystem II. *Science*, *353*(6302), aaf9178. https://doi.org/10.1126/science.aaf9178
- Jeanjean, R., Zuther, E., Yeremenko, N., Havaux, M., Matthijs, H. C. P., & Hagemann, M. (2003). A photosystem 1 psaFJ-null mutant of the cyanobacterium Synechocystis PCC 6803 expresses the isiAB operon under iron replete

- conditions [https://doi.org/10.1016/S0014-5793(03)00769-5]. FEBS Letters, 549(1-3), 52-56. https://doi.org/https://doi.org/10.1016/S0014-5793(03)00769-5
- Karapetyan, N. V., Holzwarth, A. R., & Rögner, M. (1999). The photosystem I trimer of cyanobacteria: molecular organization, excitation dynamics and physiological significance. *FEBS Letters*, *460*(3), 395-400. https://doi.org/https://doi.org/10.1016/S0014-5793(99)01352-6
- Kardinaal, W. E. A., Tonk, L., Janse, I., Hol, S., Slot, P., Huisman, J., & Visser, P. M. (2007). Competition for Light between Toxic and Nontoxic Strains of the Harmful Cyanobacterium <i>Microcystis</i>
 i>. Applied and Environmental Microbiology, 73(9), 2939-2946. https://doi.org/doi.10.1128/AEM.02892-06
- Kurashov, V., Ho, M.-Y., Shen, G., Piedl, K., Laremore, T. N., Bryant, D. A., & Golbeck, J. H. (2019). Energy transfer from chlorophyll f to the trapping center in naturally occurring and engineered Photosystem I complexes. *Photosynthesis Research*, *141*(2), 151-163. https://doi.org/10.1007/s11120-019-00616-x
- Rippka, R., Deruelles, J., Waterbury, J. B., Herdman, M., & Stanier, R. Y. (1979).

 Generic Assignments, Strain Histories and Properties of Pure Cultures of Cyanobacteria. *Microbiology*, *111*(1), 1-61.

 https://doi.org/https://doi.org/10.1099/00221287-111-1-1
- Schluchter, W. M., Shen, G., Zhao, J., & Bryant, D. A. (1996). Characterization of psal and psaL Mutants of Synechococcus sp. Strain PCC 7002: A New Model for State Transitions in Cyanobacteria. *Photochemistry and Photobiology*, *64*(1), 53-66. https://doi.org/https://doi.org/10.1111/j.1751-1097.1996.tb02421.x
- Shen, G., Canniffe, D. P., Ho, M. Y., Kurashov, V., van der Est, A., Golbeck, J. H., & Bryant, D. A. (2019). Characterization of chlorophyll f synthase heterologously produced in Synechococcus sp. PCC 7002. *Photosynth Res*, *140*(1), 77-92. https://doi.org/10.1007/s11120-018-00610-9
- Whitton, B. A. (2012). Ecology of cyanobacteria II: their diversity in space and time.
- Wolf, B. M., & Blankenship, R. E. (2019). Far-red light acclimation in diverse oxygenic photosynthetic organisms. *Photosynthesis Research*, *142*(3), 349-359. https://doi.org/10.1007/s11120-019-00653-6
- Zhao, C., Gan, F., Shen, G., & Bryant, D. A. (2015). RfpA, RfpB, and RfpC are the Master Control Elements of Far-Red Light Photoacclimation (FaRLiP) [Original Research]. Frontiers in Microbiology, 6. https://doi.org/10.3389/fmicb.2015.01303
- Zhao, Y., Shi, Y., Zhao, W., Huang, X., Wang, D., Brown, N., Brand, J., & Zhao, J. (2005). CcbP, a calcium-binding protein from <i>Anabaena</i> sp. PCC 7120, provides evidence that calcium ions regulate heterocyst differentiation. *Proceedings of*

the National Academy of Sciences, 102(16), 5744-5748. https://doi.org/doi:10.1073/pnas.0501782102



Appendix FRL-WT 438 1.4 Normalized absorbance (a.u.) FRL-psaF2 FRL-psal2 1.2 FRL-psaJ2 FRL-psaL2 1.0 8.0 624 0.6 679 0.4 710

Appendix 1 Absorbance spectra of the mutants and WT cells grown under FRL Absorbance spectra of the FRL Syn7335-WT and the mutants' (psaF2-, psaI2-, psaJ2-, and *psaL2*⁻) cells normalized to 0-1 and then normalized to the pick point of 679nm.

560

Wavelength (nm)

640

720

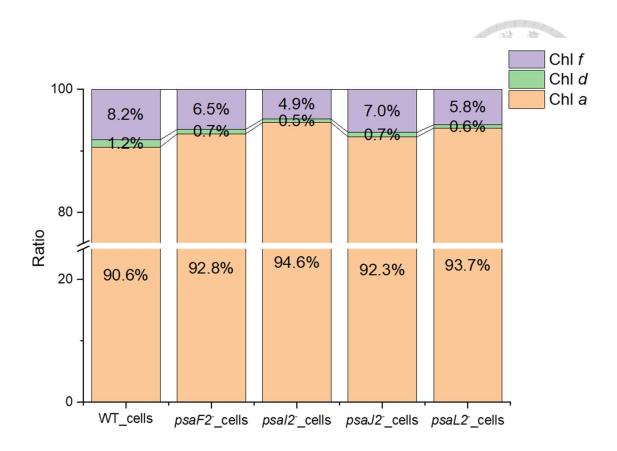
800

0.2

0.0

400

480



Appendix 2 The chlorophyll ratio of Chl a: Chl d: Chl f in the 100 % stacked bar chart of FRL Syn7335-WT, psaF2-, psaI2-, psaJ2-, and psaL2- cells

The cells of the mutants ($psaF2^-$, $psaJ2^-$, $psaJ2^-$, and $psaL2^-$) were grown under FRL with ~100 µmol photons m⁻² s⁻¹ (centered at 730 nm). In contrast, the FRL Syn7335-WT cells were grown under FRL with ~50 µmol photons m⁻² s⁻¹ (centered at 730 nm) and had a higher FRL to WL ratio, and were acclimated to FRL more completely.